OPTIMIZATION AND ASSESMENT OF SHAPE, ALIGNMENT, AND STRUCTURE OF InP/InGaAsP WAVEGUIDE VERTICALLY COUPLED OPTICAL ADD-DROP MULTIPLEXERS

Maura Raburn, Katharina Rauscher, Yae Okuno, Nadir Dagli, and John E. Bowers

Electrical and Computer Engineering Department
University of California, Santa Barbara, CA 93106
This work is supported by Walsin Lihwa Corporation.

Abstract

An investigation of optimal waveguide layout shapes for vertically-coupled, wafer-bonded InP/InGaAsP optical add-drop multiplexers has been performed through integration of the coupled-mode Ricatti equation, providing potential sidelobe levels of less than –32 dB and filter bandwidths over 20% narrower than those of previous devices. Effects of non-ideal processing conditions on filter performance are analyzed as well.

I. Introduction

As photonic circuits become more complex, multi-layer integration of interconnects becomes important to overcome the limitations of substrate size and difficulty in connecting a large number of input and output fibers or wires. By making the leap to multi-layer interconnects, more compact devices can be obtained and further creativity in circuit design is afforded. Also, because different types of devices (lasers, detectors, switches, etc.) are often best made with different materials, methods of integrating different materials onto a single chip must be addressed. Finally, some devices can be made smaller when vertical integration, rather than lateral integration, is employed. Three-dimensional routing of signals will thus be very advantageous for significantly more compact and powerful photonic ICs.

Other technologies for fabricating 3D photonic integrated circuits (PICs) include that of bonded vertically coupled micro-ring resonators [1], micro-optoelectronic mechanical systems (MOEMS) devices [2], and photonic crystals [3]. We have chosen a direct-contact wafer bonded vertically coupled InP/InGaAsP waveguide arrangement to allow device operation over a broad range for wavelength division multiplexing (WDM) applications and compatibility with other material systems and devices.

An analysis of the optimum waveguide layout shape for vertically coupled waveguides in terms of filter bandwidth and sidelobe levels has yet to be reported in detail. Optical add-drop multiplexers (OADMs) for the 1550-nm range are chosen as a focus because they are key channel routing components in wavelength-division multiplexed systems. An analysis of the effect of non-ideal processing (misalignment of waveguide layers, non-ideal growth) on the filtering ability of coupled guides is also useful for practical implementation of this technology.

II. Device Fabrication and Structure

InP/InGaAsP waveguides are chosen as a focus because of the range of active InP-based devices that could be combined with this technology. The simulations could be applied to other material systems, or a combination of material systems (InP/GaAs, Si/InP, GaN/GaAs, etc.), through a modification of the indices of refraction of the structure for ease of integrating diverse devices. Using bonded devices that couple vertically, a large number of photonic IC planar layers of various compositions are possible, allowing for new possibilities in PIC architecture.

The processing procedure begins with the metal-organic chemical vapor deposition (MOCVD) growth of a 0.2-μm InGaAs etch stop, 0.8-μm InP layer, 15-nm InGaAsP etch stop, 0.2-μm InP cladding layer, 1-μm InGaAsP (λ_g=1.066μm) guiding layer, 1.5-μm InP cladding and support layer, 0.22-μm InGaAsP (λ_g=1.359μm) guiding layer, 0.4-μm InP cladding layer, 15-nm InGaAsP etch stop, and 0.8-μm InP layer on a (001) InP substrate.

The bottom waveguides are fabricated first because the bonding and substrate removal steps in effect reverse the epitaxial growth order. Waveguide ridges are defined in the InP ridge layer using methane-hydrogen-argon reactive ion etching with SiN masking. Another round of SiN masking and etching of the InP cladding and InGaAsP waveguide core is then performed to prevent coupling from guided mode of the top waveguide to the slab mode of the bottom waveguide and vice versa. The patterned sample and a blank unpatterned sample of InP are then cleaned thoroughly, assembled in methanol, and bonded at 630°C in a nitrogen atmosphere for 50 minutes. No alignment is required during the assembly because only one of the two samples is patterned. The substrate and etch stop layer of the patterned sample are then removed via wet etching. Processing of the next layer of waveguides is the same as that for the previous except that infrared (IR) photolithography is used to align the "top" waveguide layer mask to the previously created "bottom" waveguides. Lastly, the sample is cleaved and anti-

0-7803-7320-0/02/$17.00©2002IEEE

reflection (AR) coated. The OADM layout is shown in Figure 1 and the cleaved output facet before AR coating is shown in Figure 2.

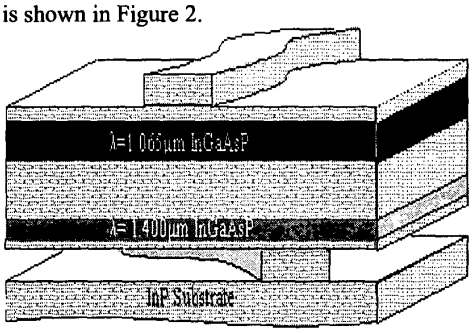

Fig. 1. Layout of OADM.

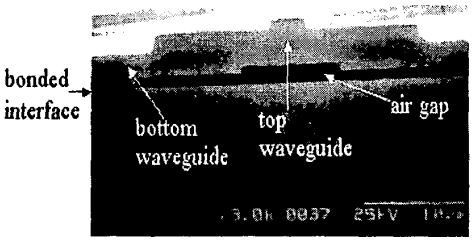

Fig. 2. Cleaved output facet of OADM before AR coating.

III. Device Design

The optimal design of OADM device mask layout includes the reduction of sidelobe levels. Parallel waveguides have prohibitively high sidelobes that often prevent them from being used as effective filters. Substantial improvement in the drop port sidelobe levels are observed with the transition from parallel to crossed x-shaped waveguides [4]. Further improvement is possible, and this section analyzes the theoretical approach. Let R and S be defined as the complex amplitudes of the incident and coupled waves in the device. The relationship between R and S for codirectional coupling takes the form of a single nonlinear Ricatti equation where S and R are expressed in terms of a variable ρ (defined as their ratio multiplied by a phase factor) [5, 6]:

$$\frac{d\rho}{dz} = -j\left(2\delta + \frac{d\phi}{dz}\right)\rho + j\kappa(\rho^2 - 1), \qquad (1)$$

where

$$\rho = \frac{S}{R}e^{-j\phi}. \qquad (2)$$

Here κ is the coupling coefficient, φ is a measure of the spatial variation in the phase matching condition, and z is the coordinate in the propagation direction. δ is a measure of the deviation of the wavelength of operation from the center wavelength for which the device was designed to couple 100%:

$$\delta = \frac{2\pi}{\lambda}(n_{eff1} - n_{eff2}). \qquad (3)$$

$n_{eff1/2}$ is the effective index of the top/bottom waveguide. The coupled-mode equation (1) can be numerically integrated over the device length to find ρ at the device output. A fourth-order Runge-Kutta integration is used because of accuracy and ease of implementation.

When little power is coupled (ρ << 1), the solution of the above Ricatti equation becomes much simpler. For this case, a Fourier transform relation exists between ρ and the coupling coefficient κ [6]:

$$\rho\left(-\frac{L}{2}\right) = -je^{-j(\phi+\delta L)}\int_{-\frac{L}{2}}^{\frac{L}{2}}\kappa(z)e^{-j(2\delta z-\phi)}dz, \qquad (4)$$

where L is defined as the device length. Fourier transform simulations were performed to corroborate the Ricatti equation numerical integration solution for low coupled powers.

Using either of the two approaches, the filter response in terms of the fraction of input power coupled to the drop port can be found by noting that:

$$\frac{P_{coupled}}{P_{input}} = \frac{|S^2|}{|S^2|+|R^2|} = \frac{|\rho^2|}{|\rho^2|+1}. \qquad (5)$$

Thus, we have two methods to relate coupled power to coupling coefficient κ: integration of (1) or evaluation of (4).

To find the bandwidth, sidelobes, and pass band shape for coupling corresponding to any arbitrary function, we set κ(z) equal to the function multiplied by a factor dependent on the number of times coupling back and forth over the length (3 for these simulations, as the OADMs are designed to couple light multiple times from input to drop waveguide over the device length for narrower bandwidths), the device length L, and a normalization term. One can then determine the passband shape in the frequency domain of a device with this κ(z) by calculating the coupled power using (1) or (4) over the wavelength deviation (δ) range of interest. κ can be calculated for a particular waveguide spacing using the finite difference technique to determine the mode profiles of the top and bottom waveguides and integrating over the dot product of the profiles [7]. In this manner, κ can be found for any waveguide spacing and hence the waveguide layout and device length for any κ(z) can be determined.

Many functions from filter theory [8] were compared in terms of bandwidth, sidelobe level, and device length using both the 4-th order Runge-Kutta integration and Fourier transform analysis. The results are shown in Figure 3.

Name	Taper Function	-20dB half width	peak first min	side-lobe	Length
Modified Blackman	1+1.125cos(2πz/L)+ 0.183cos(4πz/L)	7.5nm	9.1nm	-32.4dB	4001μm
Adjusted Hamming	1+0.93cos(2πz/L)	6.5nm	7.5nm	-22.3dB	3718μm
Gaussian	exp(-π4.25z²/L²)	6.3nm	7.6nm	-31.5dB	4011μm
X, θ=0.3°	Straight crossing wgs	7.4nm	8.5nm	-26dB	4000μm
Kaiser γ=10	$\frac{\gamma}{\sinh(\gamma)} I_0\left[\gamma\sqrt{1-\left(\frac{2z}{L}\right)^2}\right]$	8.5nm	9.6nm	-27.2dB	3793μm
Raised Cos	1+ cos(2πz/L)	9.1nm	6.5nm	-18.7dB	4277μm
Hamming	1+ 0.852cos(2πz/L)	5.9nm	6.8nm	-24.9dB	3960μm
Blackman	1+1.19cos(2πz/L)+ 0.19cos(4πz/L)	7.5nm	8.5nm	-23.3dB	4000μm
Butterworth N=3 zc=0.185L	$\frac{1}{\sqrt{1+\left(\frac{z}{z_c}\right)^{2N}}}$	11.5nm	12.5nm	-23.9dB	3904μm
Chebychev N=3, ε= 2, zc=0.17L	$\frac{1}{\left\lvert 1+\varepsilon^2\left(\cos\left(N\arccos\left(\frac{z}{z_c}\right)\right)\right)^2\right\rvert}$	18.6nm	12.3nm	-14.2dB	3492μm
Parallel wg	1	92.9nm	9.2nm	-4.4dB	1927μm
Windowed Sinc, b=3/L	sin(2bz)/z (1+0.93cos(2piz/L))	8.1nm	9.3nm	-26.3dB	3653μm
Sinc, b=3/L	sin(2bz)/z	11.4nm	7.1nm	-14.4dB	3126μm

Fig. 3. –20dB half width, first minima of central peak, and magnitude of first sidelobe for various taper functions using 4th order Runge-Kutta numerical integration of coupled-mode Ricatti equation. L denotes device length.

All devices except the parallel waveguides were designed to completely couple light back and forth three times between the input and drop waveguides, with at least 10μm separation between guides at the device edges. 10μm was found to be a sufficient separation between guides to reduce the coupling to zero. The parallel waveguides were simulated to have no lateral separation. These conditions were used instead of a requirement that the devices be the same length because otherwise many devices would be much longer than necessary. It is worth noting that sidelobe levels of less than –32 dB and filter bandwidths over 20% narrower than those of the previous x-crossing devices are possible with certain coupler shapes.

The device simulations for which κ(z) is set proportional to Gaussian, adjusted Hamming, and modified Blackman functions were judged to be the best based on sidelobe levels, filter bandwidths, and device length. Gaussian and modified Blackman had the lowest sidelobes of all functions simulated, less than –30dB. Adjusted Hamming is hundreds of microns shorter than most of the other devices with reasonable bandwidths and sidelobes.

Preliminary results are shown in Figure 4, though processing challenges still remain. More comprehensive data will be presented at the conference.

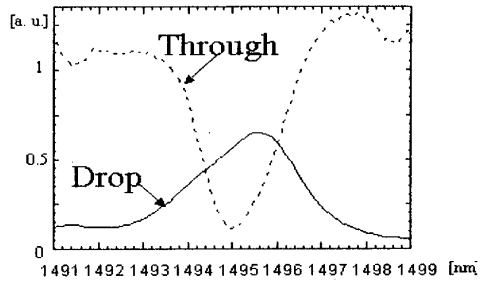

Fig. 4. Preliminary wavelength scan of through and drop ports of device with κ(z)μGaussian

A comparison of the filter performance for the 4th order Runge-Kutta integration, Fourier transform, and beam propagation method (BPM) [9] are shown in Figure 4. The three approaches show reasonable agreement for small deviations from the center wavelength. The fast, and easy-to-compute Fourier transform relation is thus considered to work well to obtain a quick approximation for small δ. The BPM and the Runge-Kutta integration approaches are both considered "actual" solutions. The difference between the two "actual" solutions is due to time and memory limitations of grid spacings and step sizes in the computations. The BPM involves a huge number of calculations as the light is simulated to traverse the device step by step with very small step size. Thus, for small coupled powers, a very large number of significant figures must be retained to avoid round-off errors. This is why the BPM curve is not smooth for large wavelength deviations where coupling is low.

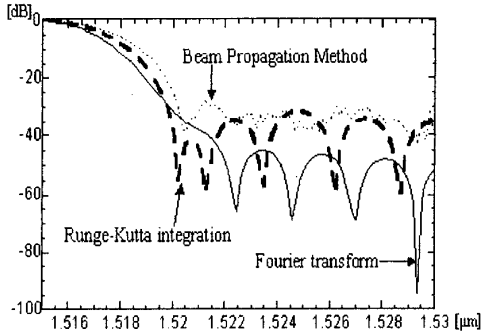

Fig. 5. Comparison of OADM performance (coupled power vs. wavelength) for coupler for which κ(z)∝Gaussian with 4th order Runge-Kutta numerical integration of the Ricatti equation, Fourier transform, and beam propagation method analyses.

IV. Non-Ideal Processing Conditions

One new concern for vertically coupled waveguide devices is waveguide alignment. Traditional horizontally coupled devices are more sensitive to waveguide spacings but also typically require only one

mask layer for patterning the guides so alignment has not been an issue. Little has been reported regarding such recent vertical coupling alignment concerns.

The Gaussian waveguide layout from above was used in the simulations because it had the most desirable filter characteristics overall. Vertical misalignment is not a concern because one of the two waveguides is assumed to be straight. However, lateral misalignment can lead to filter degradation and can be particularly problematic when aligning a "top" mask layer to layers hidden below the surface after bonding and substrate removal. The filter response for lateral misalignment is shown in Figure 6 a). Though a misalignment by 2μm is rather extreme, it is included to illustrate the degree of misalignment tolerated by vertically coupled waveguide devices. Thus, we note that device performance is not greatly compromised by misalignments on the order of 1μm or less.

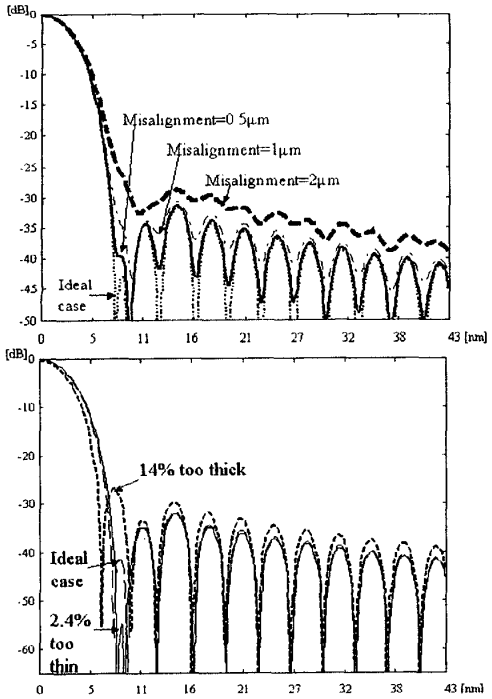

Fig. 6. Coupled power vs. wavelength for coupler for which $\kappa(z) \propto$ Gaussian a) when laterally misaligned by 0.5, 1, and 2μm, and b) when the thinner, higher index guiding layer is grown to the wrong thickness. The waveguides are 3um wide.

Through backside illumination, misalignments of less than 0.5μm can be obtained with IR photolithography. However, it can be difficult to measure the misalignment of the "top" and "bottom" mask layers with this technique after the patterning is completed. A more precise alignment method consists of etching alignment marks through most of the epitaxial layers before bonding such that the marks are visible on the other side of the epitaxial layer after bonding and substrate removal [10]. In this way, verniers to measure misalignment can be included so that the actual effects of the misalignment can be simulated [11].

Another potential obstacle to realizing a device as designed is imperfect epitaxial layer growth. Operating wavelengths and filter bandwidths can change significantly if layers are grown of the wrong thickness or composition. It is useful to simulate from the parameters of a non-ideal growth the required alteration to waveguide widths and heights for desired device operation in order to change them if possible before processing. Results are shown for a guiding layer grown too thick and too thin in Figure 6 b). One can see that sidelobe levels may increase greatly with only a small difference in waveguide thickness. Devices made from material of undesirable composition can be simulated in a similar manner.

For accuracy and speed, the 4th order Runge-Kutta integration of the Ricatti coupled mode equation was used for all misalignment and non-ideal growth simulations.

V. Conclusions

Sidelobe levels less than –32dB have been simulated by tailoring the waveguide shapes. Experimental testing is underway. The effects of non-ideal processing conditions have also been examined. Through combining many efforts, multi-channel OADMs of low bandwidth and sidelobe levels tuned through the carrier injection effect will be possible.

References

[1] D. V. Tishinin *et al.*, *IEEE Photon. Technol. Lett.*, vol.11, (no.8), IEEE, Aug. 1999, pp. 1003-5.

[2] M. Wu, *Proceedings of the IEEE*, vol. 85, (no. 11), November 1997, pp.1833-1856.

[3] A. Chutinan *et al.*, *Appl. Phys. Lett.*, vol.79, (no.17), AIP, 22 Oct. 2001, pp.2690-2.

[4] B. Liu *et al.*, "Optical Add/Drop Multiplexers Based on X-Crossing Vertical Coupler Filters", *IEEE Photon. Technol. Lett.*, vol. 12, (no. 4), April 2000, pp. 410-412.